GEM TN-93-307

A Prototype Silicon Preradiator for the SSC

A. Arodzero, J. Brau, R. Frey, K. Furuno, H. Hwang,
D. Mason, D. Strom, X. Yang - University of Oregon
G. Bashindzhagyan - Moscow State University
R. A. Todd - Oak Ridge National Laboratory

February 1993

Abstract:

We describe the design and first results from the test of a prototype of a preradiator detector. Such a detector could be used to enhance the identification of photons and electrons at the Superconducting Super Collider (SSC). Specifically, it may be used by the GEM detector to distinguish between single photons from Higgs decay and background photon pairs from π^0 decay. Our prototype consists of tungsten radiator followed by silicon strip detectors. The tungsten thickness was changeable, varying from 0 to 3 radiation lengths. Two silicon detectors, oriented in X and Y, consist of 48 strips, each of length 48mm. The pitch is 1mm. This granularity is required for separating single and multi-photons at the SSC. The readout is achieved by low-noise, low-power custom preamplifier chips mounted directly on the detectors via custom circuit boards. This preradiator was tested in a beam at Brookhaven (BNL) in July 1992. A lead glass array placed behind the silicon was used to determine energy resolution effects. The results from the test on spatial distributions and energy resolution, including correction for the energy deposited in the preradiator are presented, along with comparisons to EGS simulations.

A Prototype Silicon Preradiator for the SSC

A. Arodzero, J. Brau, R. Frey, K. Furuno,
H. Hwang, D. Mason, D. Strom, X. Yang,
Physics Department,
University of Oregon, Eugene, OR 97403
G. Bashindzhagyan,
Moscow State University, Russia
and R.A. Todd,
Oak Ridge National Laboratory,
Oak Ridge, TN 37831

Abstract

We describe the design and first results from the test of a prototype of a preradiator detector. Such a detector could be used to enhance the identification of photons and electrons at the Superconducting Super Collider (SSC). Specifically, it may be used by the GEM detector to distinguish between single photons from Higgs decay and background photon pairs from π^0 decay. Our prototype consists of tungsten radiator followed by silicon strip detectors. The tungsten thickness was changeable, varying from 0 to 3 radiation lengths. Two silicon detectors, oriented in X and Y, consist of 48 strips, each of length 48mm. The pitch is 1mm. This granularity is required for separating single and multi-photons at the SSC. The readout is achieved by low-noise, low-power custom preamplifier chips mounted directly on the detectors via custom circuit boards. This preradiator was tested in a beam at Brookhaven (BNL) in July 1992. A lead glass array placed behind the silicon was used to determine energy resolution effects. The results from the test on spatial distributions and energy resolution, including correction for the energy deposited in the preradiator are presented, along with comparisons to EGS simulations.

1 Introduction

The potential of lepton and single-γ identification as physics tags motivates the deployment of a preradiator at the SSC. Numerous physics goals benefit from this subsystem: heavy Higgs, intermediate mass Higgs, top searches and studies, direct photon production, as well as more exotic studies such as Z' and heavy quarks. The excellent electron identification and π^0 rejection of the preradiator could contribute significantly to these physics studies. Most significant for the GEM detector[1] is the role of the preradiator for enhancing the $H \rightarrow \gamma\gamma$ signal for a Higgs boson of intermediate mass. The preradiator would help to distinguish between single photons (from $H \rightarrow \gamma\gamma$) and photon pairs from π^0 decay in (background) multi-jet events.

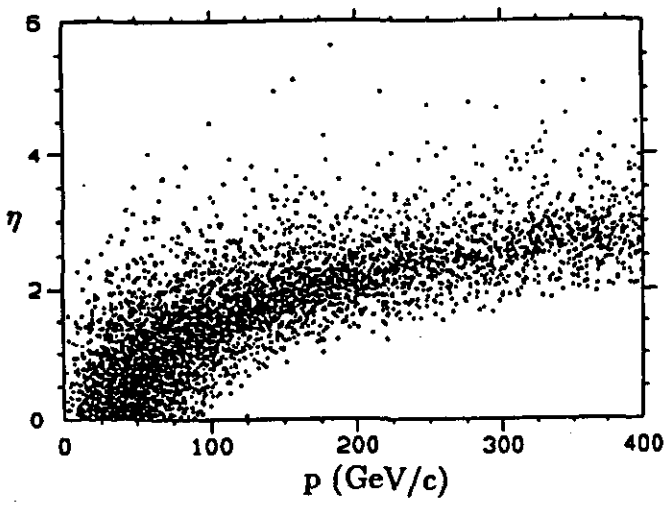

Figure 1: Pseudorapidity (η) versus photon energy for $H \rightarrow \gamma\gamma$ events at the SSC for $m_H = 100$ GeV/c^2.

The pixel structure of a silicon strip preradiator offers important advantages over other techniques in electron/hadron rejection. The overlap of complicated events, for example, is much simplified with a pixel detector. A "pixel" here is formed by crossed layers (X and Y) of silicon strips, where each strip has a rectangular shape with dimensions of approximately 1 mm × 50 mm. Such a preradiator could determine the centroid of an electromagnetic shower with a precision of better than 0.5 mm in both transverse coordinates. In the early stages of shower buildup the transverse spread of the electromagnetic cascade about the incoming particle direction is limited to a small fraction of the Moliere radius that describes the ma-

*This work was supported by the U.S. Department of Energy under contract No. DE-FG06-85ER40224 and by the Texas National Research Laboratory Commission project number RGFY92-119.

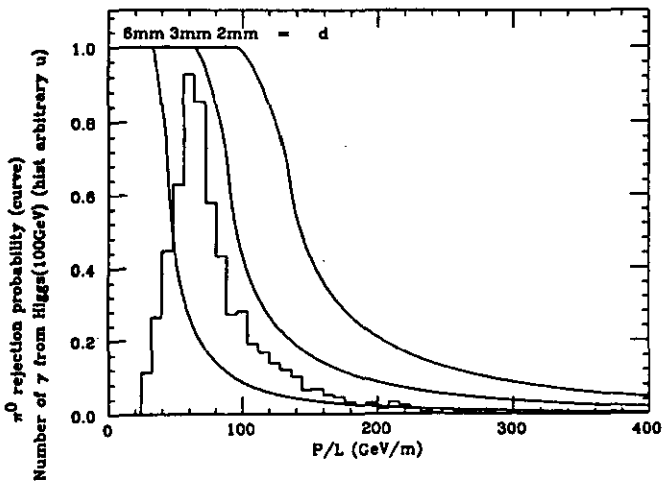

Figure 2: Curves: π^0 rejection efficiency assuming that the photon showers can be distinguished at a distance $d = 2, 3, 6$ mm, as a function of p/L, where p is momentum and L is path length. Histogram: Photon energy distribution from $H \rightarrow \gamma\gamma$ as seen by a GEM preradiator.

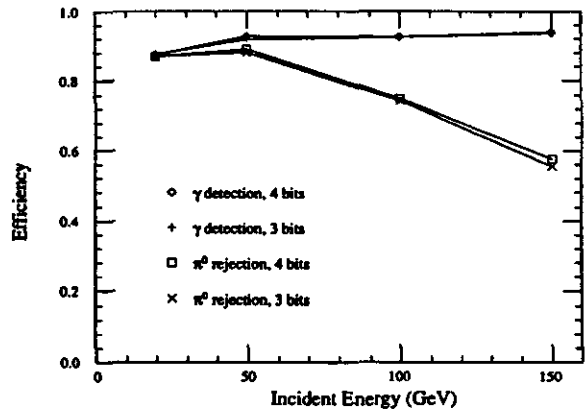

Figure 3: Efficiency for π^0 rejection or photon detection as a function of energy, based on EGS simulation. The detected energy have been digitized with 3 or 4 bits, as indicated.

ture cascade. This tight energy cluster, having full width ≈ 2 mm after 3 X_0 of tungsten, is an important signature of a photon or electron. It also serves to aid in isolating electron candidates within a jet. Projective devices, for example, have more trouble with hadron/photon pileup within a jet. A two-dimensional measurement will give maximum rejection power.

A more quantitative understanding of preradiator requirements for the $H \rightarrow \gamma\gamma$ signal has been obtained. First, we show in Fig. 1 a scatter plot of pseudorapidity (η) versus photon energy for $H \rightarrow \gamma\gamma$ events at the SSC for $m_H = 100$ GeV/c^2. We see that it is most important to cover the central region ($|\eta| < 1.5$), where the photon energy is relatively small. The histogram of Fig. 2 is this photon energy distribution as seen by a GEM preradiator at radius 75 cm in the barrel of the detector and total coverage $|\eta| < 2.5$. This indicates which photon energies are important for $\pi^0 \rightarrow \gamma\gamma$ rejection, as well as $H \rightarrow \gamma\gamma$ detection. The histogram is actually given as a function of p/L, where L is the distance from interaction point to preradiator element. The $\gamma\gamma$ opening angle from π^0 decay scales as p/L. The curves give the π^0 rejection probability assuming that the photon showers can be distinguished at a distance $d = 2, 3, 6$ mm. One sees that a value $d \leq 3$ mm would give good rejection over the relevant energy range. (We note that during preparation of this paper the GEM collaboration was considering an increase of the inner tracker radius, which would move the preradiator radius in the barrel from 75 cm to $\approx$ 100 cm. For a given detector granularity, this would further increase the rejection probability in the barrel region.)

As mentioned earlier, the narrow width of electromagnetic showers after a few radiation lengths of high-Z radiator allow nearby showers to be distinguished at the ≈ 3 mm level, as required by the $H \rightarrow \gamma\gamma$ kinematics. To achieve a quantitative estimate of preradiator effectiveness, the EGS monte carlo[2] has been used to simulate single-photon and $\pi^0 \rightarrow \gamma\gamma$ showers in a silicon-strip preradiator. The primary results are shown in Fig. 3. The statistical significance for Higgs detection depends strongly on both photon detection efficiency and π^0 rejection efficiency. It depends on the relative admixture of physics background event types– γ-γ, γ-jet, and jet-jet – which is not well known. In Fig. 3 the γ detection and π^0 rejection efficiencies are given as a function of the γ or π^0 energy. The detectable energy has been digitized into 3 or 4 bits. A simple two-threshold cluster finding algorithm has been used to analyze the events.

2 Preradiator Prototype

The silicon detector diodes making up the strip preradiator are Hamamatsu type S2461. Each such detector is 48 mm $\times$ 48 mm, segmented into 48 strips of 1 mm pitch and 0.9 mm width. The silicon wafer thickness is 0.3 mm. Each strip has capacitance $\approx$15 pF. The detectors were operated at 70 volts and were fully depleted. The principle of connection is shown in Fig. 4. Note that in our case the bias voltage is positive, and is applied to the detector side opposite of the readout. This has the advantage of allowing the preamplifiers to be directly DC-coupled to the detectors. The potential disadvantage of this scheme is that an extremely high leakage current in one strip could jeopardize an entire detector. We experienced no difficulties of this type.

The preamplifier used for the strip readout [3] was a "folded cascode" design with a JFET input stage. The design is due to the Oak Ridge group as part of the SECC SSC sub-system project. The specific model employed for the strips was designated FC1X1, and was designed for a detector capacitance of $\approx$30 pF. These custom chips were

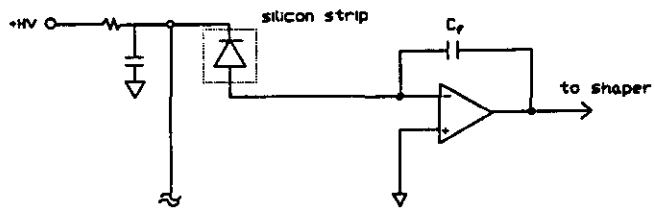

Figure 4: Principle of connection for each silicon detector element, represented here by a diode.

fabricated with four channels per 1 cm × 1 cm × 2 mm package. The feedback capacitor for the FC1X1 is 10 pF, for a sensitivity of 100 mV per pC input charge. The equivalent noise is 4500 RMS electrons at room temperature (for a 27 pF detector). The rise time is 4 ns. The power consumption is 18 mW per channel. The preamps are designed to drive signals for not much more than ≈1 m. A set of shaper/driver channels was employed for our test. These were slower, more conventional channels, also designed and built at Oak Ridge, with a shaping time of about 50 ns and a voltage gain of 40.

We note that the electronics described above was designed for silicon electromagnetic calorimetry. A preradiator-specific design would be somewhat different. The dynamic range seen by a preradiator channel is considerably smaller than a typical calorimeter channel. Hence an increased preamplifier sensitivity would be possible. And the need for large standing currents, and therefore power consumption, would be reduced in the preamplifier. A real system would include local digitization (as few as 4 bits might suffice) followed by multiplexing. Detector strips could be ganged with a connection spacing of eight or more strips. (The ambiguity would be resolved by the calorimeter information.)

Figure 5 shows the positions of silicon detectors and preamplifier chips as mounted on the readout printed circuit board. The detectors were fastened with conductive epoxy to the readout boards, thus allowing application of the positive bias voltage. The connection of the strips to the readout board was made with Al(Si) wire bonds. For mechanical stabilty, the readout board is 1 mm thick G10. The readout boards were designed to accommodate either an X or Y-strip orientation. An X-strip board and a Y-strip board were attached back-to-front to make a single rectangular unit, with the outputs from X-strip preamps and Y-strip preamps exiting the unit at opposite ends. About 80 cm of cable connected these outputs to the shaper electronics. In the test at BNL, the outputs of the shapers were passed to LeCroy Research Systems LRS FERA ADCs via 100 feet of flat ribbon cable.

Figure 6 depicts the test beam setup. One to three tungsten plates, each of thickness 1 radiation length (1 X_0 = 35mm) were placed directly before the silicon detector unit. A 3×4 -block array of lead glass, part of that previously used in BNL experiment E865, was stacked be-

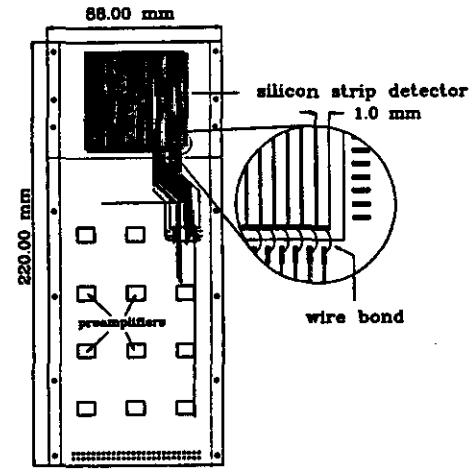

Figure 5: Drawing of a silicon detectors mounted on its readout board with preamplifier chips and output connectors. Only a few representative traces are indicated.

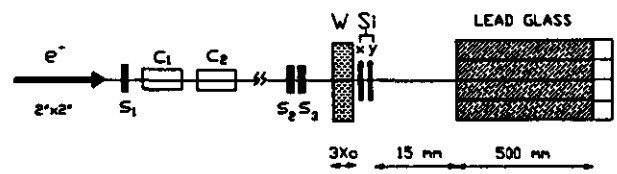

Figure 6: The test beam configuration in the A2 line at BNL. C_1 and C_2 are threshold Cerenkov for electron identification. S_1, S_2, and S_3 are plastic scintillators which provide beam timing and definition.

hind the silicon detectors. Each of the lead glass blocks had dimensions 6.4 cm × 6.4 cm × 50 cm. The lead glass blocks were readout into an LRS 2249A ADC. The electron trigger was provided by a coincidence of two upstream Cerenkov detectors and a pair of plastic scintillators just before the preradiator prototype. The data acquisiton was performed by a VME-based Motorola 167A 68040 processor.

The data taking was limited to a two day period. Data was taken at 2, 4, and 5 GeV, mostly with electron triggers, although some pion data for calibration was also taken. Our electron triggers were ≈80% pure. In addition to separate pedestal runs, pedestal events were also taken out of time with the beam spill. Data was taken with 0, 1, and 3 radiation lengths of tungsten in front of the silicon. A run was also made with 4 cm of aluminum between the preradiator and the lead glass in order to simulate the effect of a dewar wall.

Several strips were dead during data taking. We have taken these into account in the results below wherever possible. The channel-to-channel variation in the mean maximum pulse height was used as an indication of overall relative gain. The RMS of these variations were found to be ≈30% of the RMS noise. Hence no preradiator calibration was needed. Crosstalk between channels was checked in

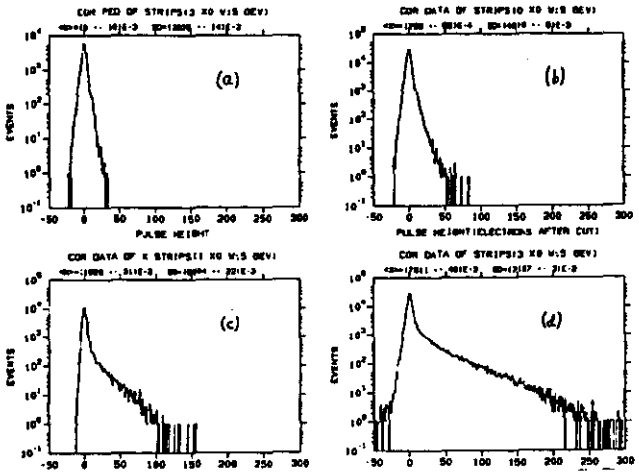

Figure 7: Pulse height distributions for all 96 strips under different conditions: (a) pedestals only; 5 GeV electrons with (b) no radiator, (c) 1 X_0 of tungsten, (d) 3 X_0 of tungsten.

the lab with alpha particles, and for the electronics alone using injected pulses. The crosstalk was found to be small, about 10% of a minimum ionizing particle (MIP), between nearest neighbor strips, and smaller still for non-nearest neighbors.

3 Preradiator Beam Test Results

The test beam results are organized below into two sections which reflect the two important questions for the physics performance of an SSC preradiator:

1. Can an electromagnetic shower be readily distinguished from nearby showers?
2. What effect does the preradiator have on the energy resolution of the electromagnetic calorimeter?

First, we present some basic distributions. Figure 7 gives the pulse height distributions for the silicon strips under different conditions. Figure 7(a) is for a pedestal run. This shows that the RMS noise is roughly 3.8 ADC counts. (It should be noted that we had to correct all the data for coherent noise pickup. Because of the shortness of time for data taking, we had little opportunity to correct the coherent pickup in the hardware, but, because of the high degree of correlation between channels, we have been able to effectively eliminate most of it offline.) This can be compared to a single MIP, which is about 10 ADC counts on average. The MIPs can, in fact, be seen in the shoulder of Fig. 7(b), which is for a run with no radiator in front of the silicon strips. Plots (c) and (d) are for runs with 1 X_0 and 3 X_0 of tungsten, respectively. One can clearly see the measurement of localized energy depositions from electromagnetic showers. Because the 5 GeV beam was the highest available to us on the A2 beam line, we focus below on the 5 GeV electron data with 3 X_0 of tungsten radiator.

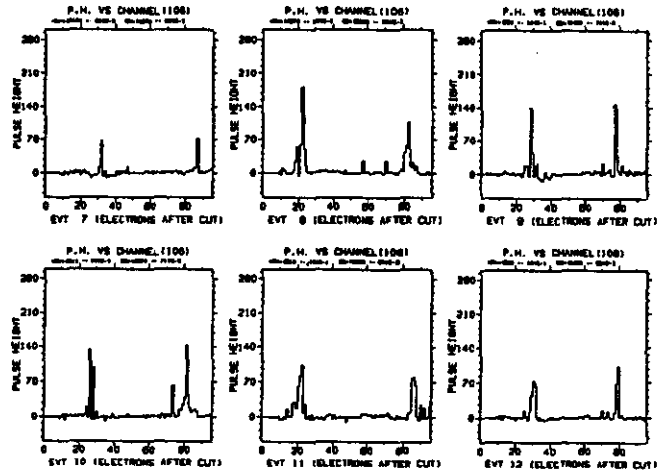

Figure 8: Event displays (pulse height versus strip number) for the first 6 events of a run with 5 GeV electrons and 3 X_0 of tungsten radiator. The X-strips are numbered 1–48, and the Y-strips are 49–96.

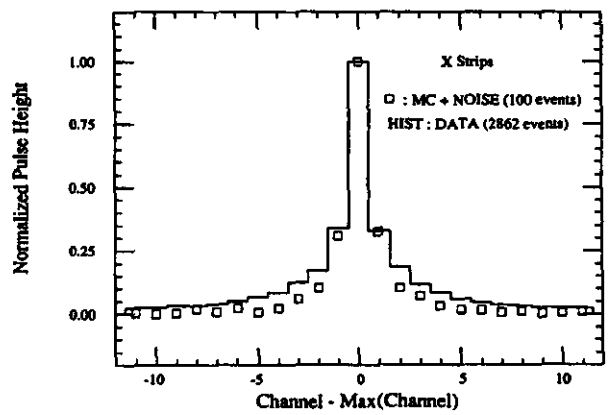

Figure 9: Transverse shower profile for X strips averaged over ≈ 2800 events for 5 GeV electrons with 3 X_0 of tungsten radiator (squares). The histogram is the corresponding EGS simulation for 100 events.

3.1 Shower Spatial Distribution

Figure 8 gives event displays for the first 6 events of a run with 5 GeV electrons and 3 X_0 of tungsten. These displays give pulse height (measured charge in ADC counts) versus strip number. One ADC count corresponds to about 13 KeV of deposited energy. One sees that while the 5 GeV electron showers are not as substantial as those expected for energies relevant for an SSC preradiator, they still appear to be reasonably well-defined in transverse profile. In lieu of a high energy electron beam, the important question is how well the 5 GeV showers can be modelled by the EGS monte carlo, and hence allow for an extrapolation to higher energy to be made with some confidence. Figures 9 and 10 are the averaged shower profiles obtained

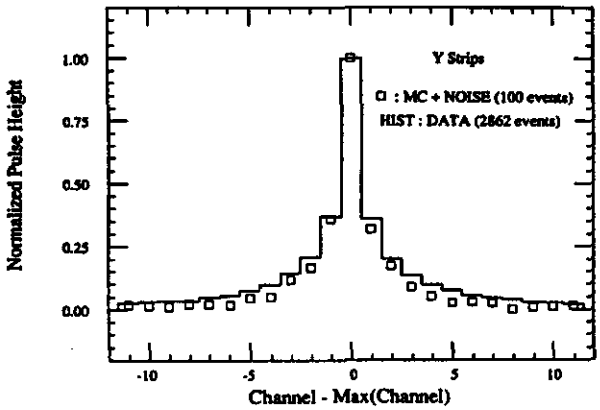

Figure 10: Same as Fig. 9 but for Y strips.

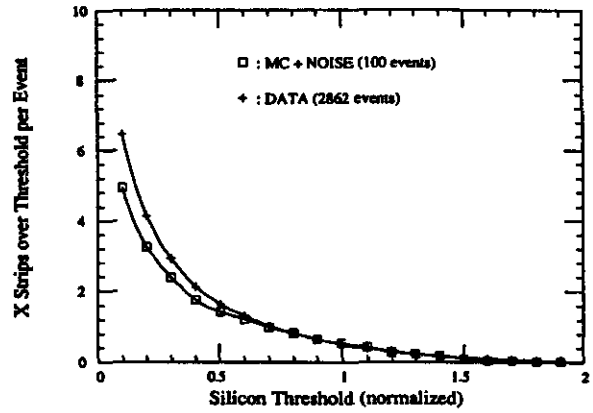

Figure 11: Distribution of number of strips over threshold as a function of that threshold for data and EGS simulation.

from the event displays by placing the strip with maximum pulse height at the center of the distribution. The squares represent about 2800 beam events, while the histograms result from the EGS simulation (100 monte carlo events). The data is normalized to the monte carlo at the center bin. One can see reasonably good agreement, but with some differences in the shoulders of the distribution. Deviations from EGS in thin-sampling detectors, specifically silicon, have been noted[4] previously. In accordance with these studies, we have taken care in the EGS description of the geometry, cutoffs (10 KeV for electrons and photons in silicon and nearby materials), and step sizes (ESTEPE option with 0.3% step in silicon and 1% elsewhere). The origin of the small deviations in transverse profile is not yet understood. We note that comparisons to EGS with this transverse granularity (1 mm) after a few radiation lengths of high-Z radiator are not commonplace.

While the average shower profiles of Figs. 9 and 10 agree well with EGS, it is also necessary to examine in detail the profiles of individual events. Since decisions from a pattern recognition algorithm used to distinguish between single showers and nearby multi-showers are based on single events, it is also desirable to examine in detail the profiles of individual events. Figure 11 shows the number of strips above some threshold as a function of that threshold for both data and for the EGS simulation. The normalization is as above, with a threshold of 1 corresponding to 1.46 MeV of deposited energy in the silicon. Again there is reasonably good agreement, but with small deviations at low threshold, qualitatively consistent with those noted above.

3.2 Energy Resolution and Correction

While a preradiator may be very useful where a highly granular electromagnetic presampler is important, especially for identifying multi-particle showers as discussed above, one must decide if this benefit is outweighed by the effect of the preradiator on the overall energy resolution of the electromagnetic calorimeter. We use the present data to demonstrate that the energy deposited in the preradiator can be used to correct the calorimeter resolution in a straightforward way.

In the BNL test, the electromagnetic calorimeter consisted of a lead glass array, as described above. By taking data with no material before the lead glass, we obtained its energy resolution. Unfortunately, we did not have an opportunity to do a good block-to-block calibration of the array. Hence the energy resolution of the entire array is not better than that of the central lead glass block. Therefore we use only the central block in this discussion. Figure 12 shows the measured correlation between the silicon response and the response of the center lead glass block. The correlation between the two is used to make the energy correction:

$$E = E_0 + \langle E_W \rangle + G(E_{Si} - \langle E_{Si} \rangle) ,$$

where E and E_0 are the corrected and uncorrected lead glass energies, respectively, $\langle E_W \rangle$ is the average energy deposited in the tungsten radiator, E_{Si} is the silicon energy, and G is the slope indicated by the correlation plot in Fig. 12. All energy distributions were fit by gaussian distributions, and the resulting resolutions are given in the Table 1 below. The EGS result with no radiator is not shown, since in this case photon statistics, which is not included in the simulation, makes a substantial contribution (about 1.8%) to the resolution. However, if the estimate for the photon statisitics is included, the simulation and data agree. This contribution is negligible in the cases with radiator present.

One can see that a substantial correction can be made to the energy resolution using the preradiator information and that this correction seems to be well-modelled by an EGS simulation. One can then be reasonably confident in the EGS predictions at higher energy. Table 2 gives resolutions from EGS simulation for a full lead glass array (*i.e.* complete shower containment) for 5 GeV and 50 GeV electrons, without and with correction from the silicon.

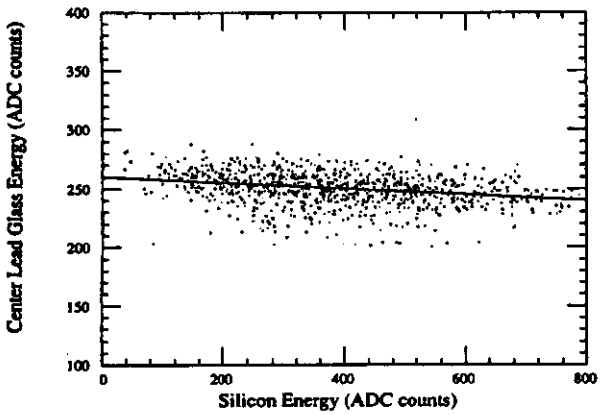

Figure 12: Scatter plot of total measured silicon energy versus measured lead glass energy. The line indicates the fitted correlation between these quantities.

Table 1
One-block lead glass resolution for 5 GeV electrons for data and EGS simulation.

	σ_E/E – Data	σ_E/E – EGS
No Preradiator	$3.2 \pm 0.1\%$	–
$3X_0$ W – no correction	$5.0 \pm 0.1\%$	$4.9 \pm 0.1\%$
$3X_0$ W – corrected	$4.2 \pm 0.1\%$	$4.0 \pm 0.1\%$

Table 2
EGS simulation results for energy resolution. Errors are 8% relative.

	σ_E/E, 5 GeV	σ_E/E, 50 GeV
$3X_0$ W – no correction	3.6%	1.1%
$3X_0$ W – corrected	2.6%	0.8%

Acknowledgements

We thank A. Carroll, D. Dayton, R. Larsen, W. Morse, and H. Takai of BNL, and W.M. Bugg of University of Tennessee.

References

[1] B. Barish, W. Willis, *et al.*,"GEM Letter of Intent", SSCL-SR-1184, SSC Laboratory, Dallas, Texas, November 1991.

[2] W.R. Nelson, H. Hirayama, and D.W.O. Rogers, "The EGS4 Code System", SLAC-Report-265, Stanford Linear Accelerator Center, December 1985.

[3] R.A. Todd, *et al.*, "Bipolar and CMOS ASIC Design for Large Physics Experiments", in *Proc. of the Conference on Electronics for Future Colliders*, LeCroy Corp., Chestnut Ridge, New York, May 1991, p. 193.

[4] G. Lindstroem, *et al.*,"MC-Simulations with EGS4 for Calorimeters with Thin Silicon Detectors", in *Proc. of the Workshop on Calorimetry for the Supercollider*, Tuscaloosa, Alabama, March 1989, p. 215.